

Review

Research Progress of Laser Additive Manufacturing Nickel-Based Alloy Metal Matrix Composites

Zhiqiang Wang^{1,2}, Shuang Gao^{1,2,*} , Shuijin Li^{1,2}, Weiguang Zhang^{1,2}, Liang Lan^{1,2}, Yifu Jiang³ and Bo He^{1,2,*} 

¹ School of Material Engineering, Shanghai University of Engineering Science, Shanghai 201620, China

² Research Center of High-Temperature Alloy Precision Forming, Shanghai University of Engineering Science, Shanghai 201620, China

³ School of Mechanical Engineering, Shenyang Institute of Engineering, Shenyang 110136, China

* Correspondence: gaoshuang_alloy@163.com (S.G.); jdhebo@163.com (B.H.)

Abstract: Nickel-based alloy metal matrix composite (NAMMC) is a new type of composite material which is expected to replace traditional Nickel-base superalloy used in the manufacture of important hot-end components in aerospace, naval ships and industrial gas turbine engines due to its excellent high temperature strength, superior thermal fatigue resistance, high oxidation resistance and thermal corrosion resistance. However, these outstanding properties make it hard to process these materials with conventional manufacturing methods such as forging and machining owing to posing problems of high cost and energy consumptions. Laser additive manufacturing (AM) with a high degree of machining freedom and a high-energy-density laser beam as heat source has been used for processing NAMMC hot-end components with superior performance and complicated structure. Nevertheless, some manufacturing defects of poor bonding, high residual stress, cracking, pore etc. still exist in laser AM NAMMC parts. Therefore, this paper reviews research progress of laser AM NAMMC at present. The control method of manufacturing defect and the effect of reinforcements on the microstructure and mechanical properties of NAMMC are summarized. In addition, the challenges and prospects of laser AM NAMMC in the future are also discussed.

Keywords: nickel-based superalloy; metal matrix composites; additive manufacturing; mechanical properties; defects



Citation: Wang, Z.; Gao, S.; Li, S.; Zhang, W.; Lan, L.; Jiang, Y.; He, B. Research Progress of Laser Additive Manufacturing Nickel-Based Alloy Metal Matrix Composites. *Metals* **2023**, *13*, 129. <https://doi.org/10.3390/met13010129>

Academic Editors: Aleksander Lisiecki and Eric Hug

Received: 29 November 2022

Revised: 23 December 2022

Accepted: 4 January 2023

Published: 9 January 2023



Copyright: © 2023 by the authors. Licensee MDPI, Basel, Switzerland. This article is an open access article distributed under the terms and conditions of the Creative Commons Attribution (CC BY) license (<https://creativecommons.org/licenses/by/4.0/>).

1. Introduction

Nickel-based alloy has excellent oxidation resistance, corrosion resistance and good mechanical properties, and can service at high temperature environments for a long time [1–4]. With the rapid development of industry in recent years, the working environment of Nickel-based alloy parts has become more and more severe, and higher requirements are put forward for the properties of high-temperature material. Nickel-based alloy metal matrix composite (NAMMC) combine the properties of matrix (toughness, formability, heat and electrical conductivity) and reinforcement (high strength, high modulus, high wear resistance and high temperature resistance). Therefore, NAMMC has better higher temperature strength and better corrosion-oxidation resistance than nickel-based alloy [5–8]. However, it is difficult to produce high-strength and complex-structure NAMMC parts with conventional manufacturing methods (forging and machining). Due to a high degree of machining freedom and a high-energy-density laser beam as heat source, laser additive manufacturing (AM) has been used for processing NAMMC hot-end components with superior performance and complicated structure. Laser AM technology includes laser beam powder bed fusion (LBPBF) [9], laser metal deposition (LMD) [10] and Laser Engineered Net-Shaping (LENS) [11]. Among them, LBPBF has a good prospect and potential. This technology uses the focused high energy laser beam to melt and solidify solid powder of a few tens of microns in diameter, layer-by-layer, under direct input from a computer-aided design system,

and finally form a three-dimensional structure of parts [12–15]. Laser AM process can be regarded as multi-layer and multi-pass welding process. So, only alloys with good welding properties are suitable to be used as the matrix for preparing full dense NAMMC with high performance. It has been reported that the comprehensive mechanical properties and forming property of laser AM NAMMCs can be improved by ceramic particle addition [16–18]. Therefore, laser AM NAMMCs are expected to replace traditional Nickel-based alloy used in important hot-end components with complicated structure in aerospace, naval ships and industrial gas turbine engines [19–23]. The choice of reinforcement is particularly important for laser AM NAMMC. The common reinforcement mainly includes carbides (SiC, TiC) [24–26], nitrides (AlN) [27,28], oxides (Al₂O₃, ZrO₂) [29,30], carbon fibers (CFs) [31], carbon nanotubes (CNTs) [32,33] and graphene nanoplatelets (GNPs) [34,35]. Ceramic particles have properties such as high hardness, high strength, high modulus and high temperature resistance. Therefore, the particle-reinforced metal matrix composites have higher specific strength, specific stiffness and heat resistance [36,37]. CFs has good resistance to high temperature oxidation and corrosion as well as self-lubricating properties. Especially, short CFs are more homogeneously distributed in the composites, so the mechanical properties of short CFs reinforced composites are isotropic [38,39]. Due to the extremely small diameter, high Young's modulus and excellent chemical stability, CNTs are used as reinforcement for lightweight and high-strength composites [40,41]. GNPs as a two-dimensional (2D) material with a high aspect ratio can improve the strength and toughness of metal matrix composites [42,43]. Adding proper amount of reinforcement particles to nickel-based alloy metal matrix can effectively improve the comprehensive mechanical properties of NAMMC. In addition, laser AM is a complex processing technology and it includes many processing parameters, such as laser beam size, laser power, scanning speed, layer thickness, and hatch spacing [44]. The optimization of process parameters is the main means to eliminate manufacturing defects, such as poor bonding, high residual stress, cracking and pore. Therefore, this also attracts much attention from researchers. At last, the reinforcement adding and process parameter adjusting impact obviously the microstructure and mechanical property of laser AM NAMMC. Therefore, this paper reviews the research progress of laser AM NAMMC from the perspective of reinforcement adding and process parameter optimizing, and their effect mechanism on the microstructure and mechanical property.

2. Reinforcement Adding

Ceramic particle reinforcement is the more common reinforcement including borides [45], carbides [46], nitrides [47], oxides [48] due to their high strength, stiffness, modulus and refractoriness. Ceramic particles reinforced NAMMCs not only has simple processing and low cost, but also exhibit the advantages of isotropy. In addition, the ceramic particles reinforced nickel matrix composites has good high temperature strength, thermal fatigue resistance, oxidation resistance and thermal corrosion resistance. The yield strength (YS), ultimate tensile strength (UTS) and elongation (EI) of NAMMCs reinforced with different ceramic particles are shown in Table 1. In addition to ceramic particle, GNPs and CNTs used as reinforcement has attracted much attention for reinforcing nickel-based alloys, owing to the high strength, high thermal and electrical conductivity [49,50]. Wang et al. [51] successfully prepared CNTs reinforced Inconel 625 composite using LBPBF technology. The results showed that the tensile strength (998 MPa) and yield strength (788 MPa) of LBPBF CNTs/IN625 were higher than the tensile strength (878 MPa) and yield strength (641 MPa) of LBPBF IN625. Chen et al. [52] successfully prepared GNPs reinforced K418 Nickel-based superalloy composites by LBPBF process. The results showed that the GNPs distributed uniformly in the matrix, and the grain of GNPs/K418 composites changed from columnar crystal to equiaxed crystal. The tensile strength (1200 MPa) and yield strength (1018 MPa) of LBPBF GNPs/K418 were higher than the tensile strength (1078 MPa) and yield strength (912 MPa) of LBPBF K418 alloy. Meanwhile, the EI of LBPBF GNPs/K418 was increased from 7.13% to 10.3%. The synchronous improvement of the strength and

plasticity was attributed to the load transfer strengthening, dislocation strengthening and Orowan strengthening. Table 2 lists the properties of common ceramic particle reinforcements [53]. The difference of physical properties between the reinforcement and the matrix should be analyzed when the reinforcement is selected, such as physical matching, interface bonding, coefficient of thermal expansion (CTE), laser absorption rate (LAR), shape and size. The influence of the reinforcement with different physical properties and geometric profile on nickel-based alloy are described in detail below.

Table 1. Mechanical properties of NAMMCs reinforced with different ceramic particles.

Reinforcement	Material	YS (MPa)	UTS (MPa)	EI (%)	Ref.
WC	Hastelloy X	590.0	780.0	37.0	[54]
	WC/Hastelloy X	670.0	850.0	32.0	
TiB ₂	Hastelloy X	555.9	692.5	6.1	[55]
	TiB ₂ /Hastelloy X	715.5	1053.2	7.2	
TiN	IN718	950.0	-	45	[56]
	TiN/IN718	1024.0	-	30	
Y ₂ O ₃	IN738	1050	1190	6.7	[57]
	Y ₂ O ₃ /IN738	1004	1148	7.2	

Table 2. The properties of common reinforcements [53].

Particals	Density ρ /(g/cm ³)	CTE α /(10 ⁻⁶ /°C)	Modulus of Elasticity E/GPa	Melting Point °C
TiB ₂	1.50	6.39	550	2980
SiC	3.21	5.40	480	2700
TiC	4.93	7.20	360	3140
WC	15.50	2.82	132	2870
AlN	3.26	4.84	310	2200
Al ₂ O ₃	3.97	6.80	460	2054

2.1. Physical Matching and Interface Bonding

The physical matching and interface bonding between the matrix and the reinforcement should be considered comprehensively when choosing the reinforcement. For instance, the lattice structure difference between TiC particles and nickel-based alloy is smaller, indicating that the better physical matching is easy to form between TiC ceramic particles and nickel-based alloy matrix. Cooper et al. [58] investigated the influences of the reinforcements with different lattice structure, such as SiC, Al₂O₃ and TiC, on IN625 Nickel-based superalloy manufactured by laser AM. The results showed that the surfaces of SiC/IN625 and Al₂O₃/IN625 composites were rough and porous, and cracks exist. However, the surface of TiC/IN625 composite was smooth and without defects. It can be seen from Figure 1 that there are many pores and large cracks in SiC/IN625 and Al₂O₃/IN625 composites, while a denser microstructure appears in TiC/IN625 composite. This indicates that TiC ceramic particle with a better physical matching is suited to be used as the reinforcement for nickel-based alloys. In addition, the good interface bonding between reinforcement and matrix is a key factor in the preparation of high density and high strength laser AM NAMMC parts. Wang et al. [59] studied the microstructure and mechanical properties of TiN reinforced IN718 composites. It can be seen from Figure 2 that the interface between TiN particles and IN718 alloy is compact, and no second phase precipitates at the interface. In addition, lots of misfit dislocations distribute near the interface, which also give rise to additional reinforcement effect. Tensile strength of TiN/IN718 composite are higher than that of IN718 alloy. Hong et al. [60] studied the interface of LMD TiC/Inconel 718 composites, and found that a interface layer with the thickness of 0.8 to 1.4 μ m formed between TiC particles and matrix, as shown in Figure 3. The interfacial layer is formed by the reaction of matrix and reinforcement into the composition of (Ti, M) C (M: Nb and Mo).

The typical metallurgical bonding interface is helpful to improve the microstructure and mechanical properties of Inconel 718 alloy.

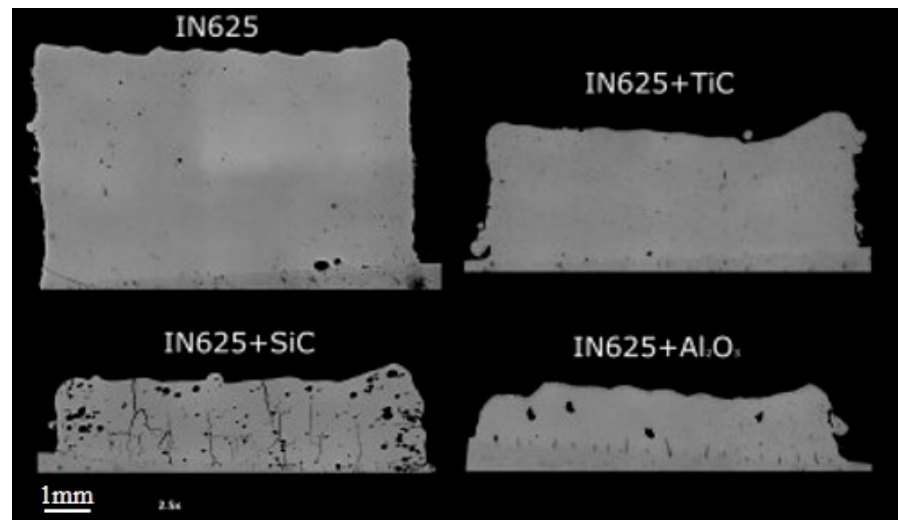


Figure 1. OM image of cross-sections of different composites [58].

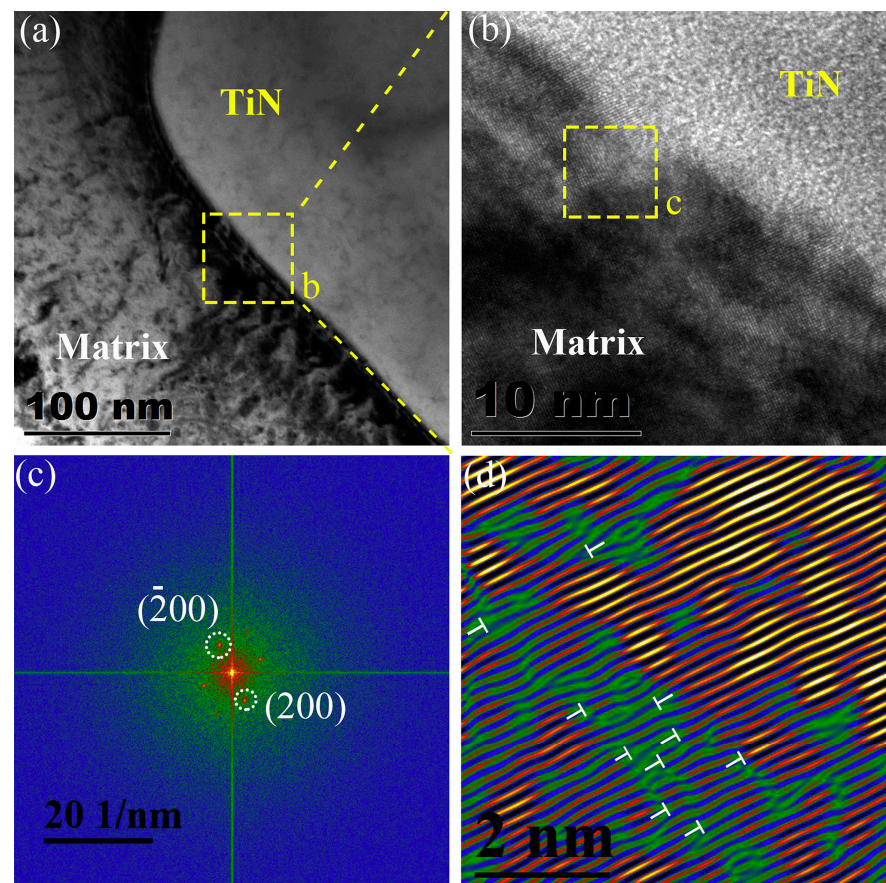


Figure 2. (a) The bright field image of the interface between TiN particle and matrix; (b) the HRTEM image of the interface between TiN particle and matrix; (c) the corresponding FFT patterns of yellow frame in (b); (d) the Inversed FFT image of (c) [59].

2.2. Coefficient of Thermal Expansion and Laser Absorption Rate

The difference of CTE and LAR between the matrix and reinforcement should be considered when selecting the reinforcement. If the CTE of reinforcement is far from that of matrix, a large amount of residual thermal stress is generated inside NAMMC parts during laser AM process, resulting in high density dislocations around the particles [53,61]. Jiang et al. [62] studied systematically TiC/Inconel 625 composite coating by laser cladding, and found that high density dislocations distributed around TiC particles (Figure 4), which was attributed to the difference in CTE between TiC particles ($7.74 \times 10^{-6}/\text{K}$) and Inconel 625 ($12.8 \times 10^{-6}/\text{K}$). Introduced residual stress increased and the cracking tendency inside NAMMC parts raised, which was not conducive to the forming property of laser AM NAMMC. In addition, the reinforcements with higher LAR can improve the forming quality of laser AM NAMMC parts. Due to the ceramic particles with higher LAR than the metal, the LAR of NAMMC is higher than that of nickel-based alloy [46,63]. The LAR of composite powders is calculated by the formula: $A = \sum \beta_i A_i$ (A_i and β_i are the LAR and the volume fraction of the powder, respectively). Table 3 lists the LAR of some metal materials, ceramics and composites [46,64]. Yang et al. [22] studied the influence of TiB_2 on the mechanical properties of Hastelloy-X. It is found from the Figure 5 that the LAR of TiB_2 /Hastelloy-X composite increases with the increase of TiB_2 content. The increase in LAR contributes to melting the composite powders and reducing the pore due to more energy from laser beam absorbed during laser AM process. The UTS of the TiB_2 /Hastelloy-X composite was 106% higher than that of Hastelloy-X. Ceramic particles can also improve the LAR of other metal alloys. For example, Li et al. [65] added TiB_2 to AlSi10Mg alloy and found that the LAR of TiB_2 /AlSi10Mg composite increased obviously. As a result, the forming quality of laser AM AlSi10Mg/ TiB_2 composite was improved and its tensile strength from 360 MPa to 530 MPa with higher EI at about 15.5%, due to the addition of TiB_2 .

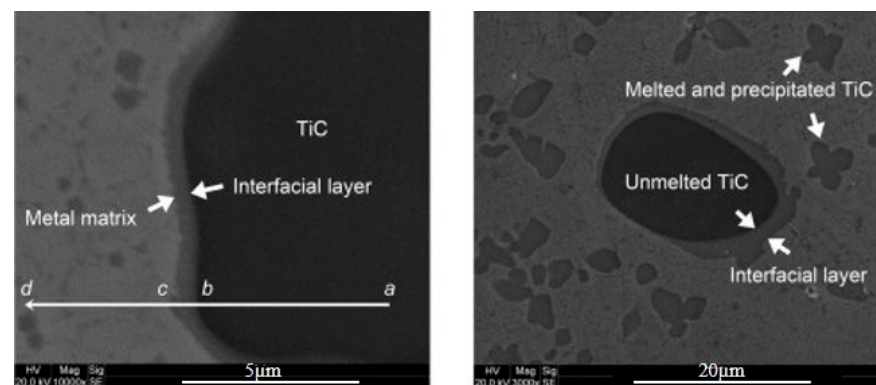


Figure 3. SEM image of the interface layer between TiC and matrix [60].

Table 3. LAR of alloys, ceramics and composites powders [46,64].

Material	Laser Absorptivity Rate (%)
Ti	0.77
Ni	0.64
Fe	0.64
Al	0.15
TiB_2	>0.71
SiC	0.78
TiC	0.82
AlSi10Mg	0.09
TiC/Inconel 718	0.72
TiB_2 /AlSi10Mg	0.71

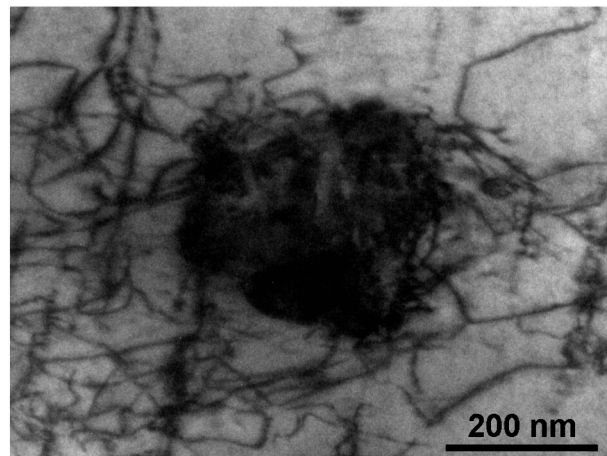


Figure 4. TEM image of dislocations around TiC particles [62].

2.3. Shape and Size

Spherical or nearly spherical particles are widely regarded as feasible reinforcements. Li et al. [66] studied the effect of spherical and non-spherical WC-reinforced on microstructure, mechanical properties and wear resistance of LMD Inconel 625 superalloy. The study showed that the wear rate of spherical WC/IN625 composite coatings was smaller than that of non-spherical WC/IN625 composite coatings. This indicated that spherical WC/IN625 composite coating had higher wear resistance. In addition, the size of the reinforcement has great influence on the mechanical properties of NAMMC [67]. Cao et al. [68] studied the effects of micron-TiC and nano-TiC on the microstructure and mechanical properties of IN625 alloy by laser AM process. The results showed that the grain of nano-TiC/Inconel 625 composite was significantly refined compared with micro-TiC/Inconel 625 composite. The hardness, tensile properties and wear resistance of the composite samples were significantly improved, and the ductility was not significantly reduced. AlMangour et al. [69] prepared micro-scale and nano-scale TiC particle-reinforced 316L stainless steel matrix by LBPBF, and analyzed the effect of ceramic particle sizes on the crack propagation of metal matrix composite. The results showed that the grain size was significantly reduced by adding nano-scale TiC. It was found that the crack propagated along the boundary of the molten pool in 316L stainless steel as shown in Figure 6A. But no cracks were found to appear inside nano-TiC/316L composite (Figure 6C), because nanoscale TiC particles were able to prevent crack propagation.

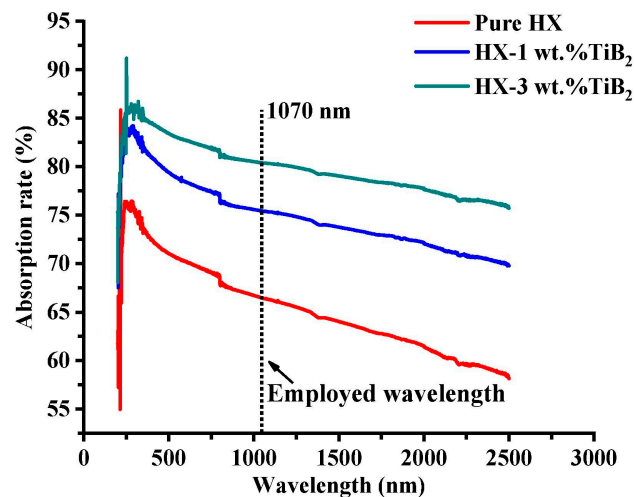


Figure 5. Diagram of laser absorption rate versus wavelength for all specimens [22].

3. Process Parameter Optimizing for Controlling Defect

The manufacturing defect of NAMMC can be reduced by optimizing the process parameters. Guo et al. [57] successfully prepared Y_2O_3 /Inconel 738 composites by LBPBF. Figure 7a shows the distribution law of pore and crack in LBPBF Inconel 738 alloy. When the laser energy density is too high or too low, a large number of pores and cracks appear in Inconel 738 alloy. When the laser power is 290 W and the scanning speed is 1200 mm/s, the forming quality of Inconel 738 alloy is the best. It indicates that optimizing the process parameters is a simple and effective method to reduce the manufacturing defect of NAMMC. Figure 7b shows the defect distribution of LBPBF Y_2O_3 /Inconel 738 composites. In addition, Guo et al. found that the Y_2O_3 particle addition significantly improved the forming quality of LBPBF Inconel 738 alloy. Zr segregation along grain boundaries was effectively eliminated and the crack density was reduced. Chen et al. [70] studied the densification behavior, microstructure evolution and wear properties of LBPBF TiC/Inconel 625 composites. Their results showed that there were many defects such as pores and non-fusion in Inconel 625 alloy when laser energy density was $139 J/mm^3$. When laser energy density reached $208 J/mm^3$, the sample density reached the highest value. Microhardness reached the maximum 440 HV. Hong et al. [67] successfully prepared LMD TiC/Inconel 625 composite with high wear resistance and high strength by optimizing process parameters. They found that some unmelted TiC particle severely agglomerated in columnar dendrites when laser energy input per unit length (LEIPUL) was below 72 kJ/m, as shown in Figure 8a,b. The columnar dendrites seriously coarsened when LEIPUL was 160 kJ/m (Figure 8d). In addition, areas 1-4 shows the EDX analysis of the chemical composition in the inter-dendrite matrix of the LMD-processed TiC/Inconel 625 composites under different LEIPUL. A large number of TiC particles melted when LEIPUL was above 100 kJ/m (Figure 8c,d) and the content of element C showed at least double increase. When LEIPUL was in the range from 72 to 100 kJ/m, TiC/Inconel 625 composite exhibited excellent microstructure and optimum mechanical properties. Wang et al. [71] studied the process optimization of oxide dispersion strengthened Nickel-based superalloy by LBPBF. Figure 9 shows the effect of process parameters on the tensile strength. Figure 9a shows that the tensile strength decreases with increasing laser power. This is because the higher the laser power, the more laser energy is input. Excessive laser energy input causes the metal powder to overmelting, resulting in more porosity and cracks in the sample during the building process. This eventually caused a decrease in the tensile strength of the sample. Figure 9b shows that the tensile strength increases first and then decreases as the scanning speed increases. The lower scanning speed will improve the temperature of melt pool, resulting in an instability of the melt pool. Excessively high scanning speed results in a low melt pool temperature, and the metal powder cannot be completely melted. Therefore, lower or higher speeds are not good for tensile strength. Figure 9c shows that the tensile strength increases first and then decreases with the increase of hatch spacing. This also indicates smaller or larger hatch spacing bring manufacturing deficiency for NAMMC, resulting in poor tensile strength.

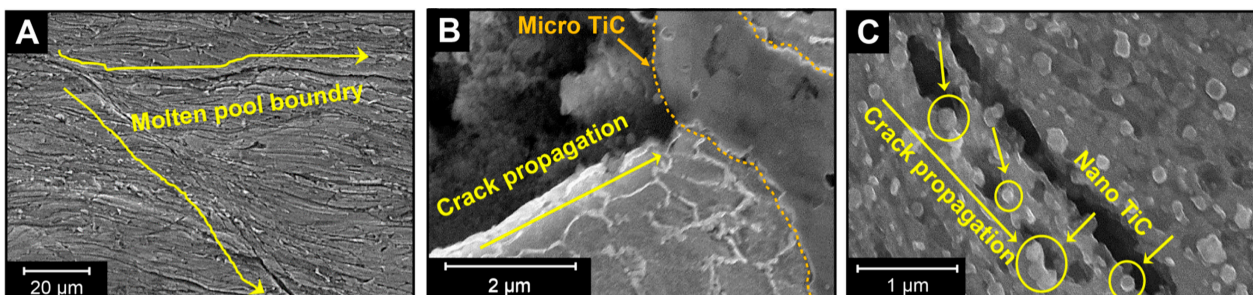


Figure 6. SEM image of crack propagation with (A) LBPBF 316L; (B) LBPBF micro-TiC/316L composite and (C) LBPBF nano-TiC/316L composite [69].

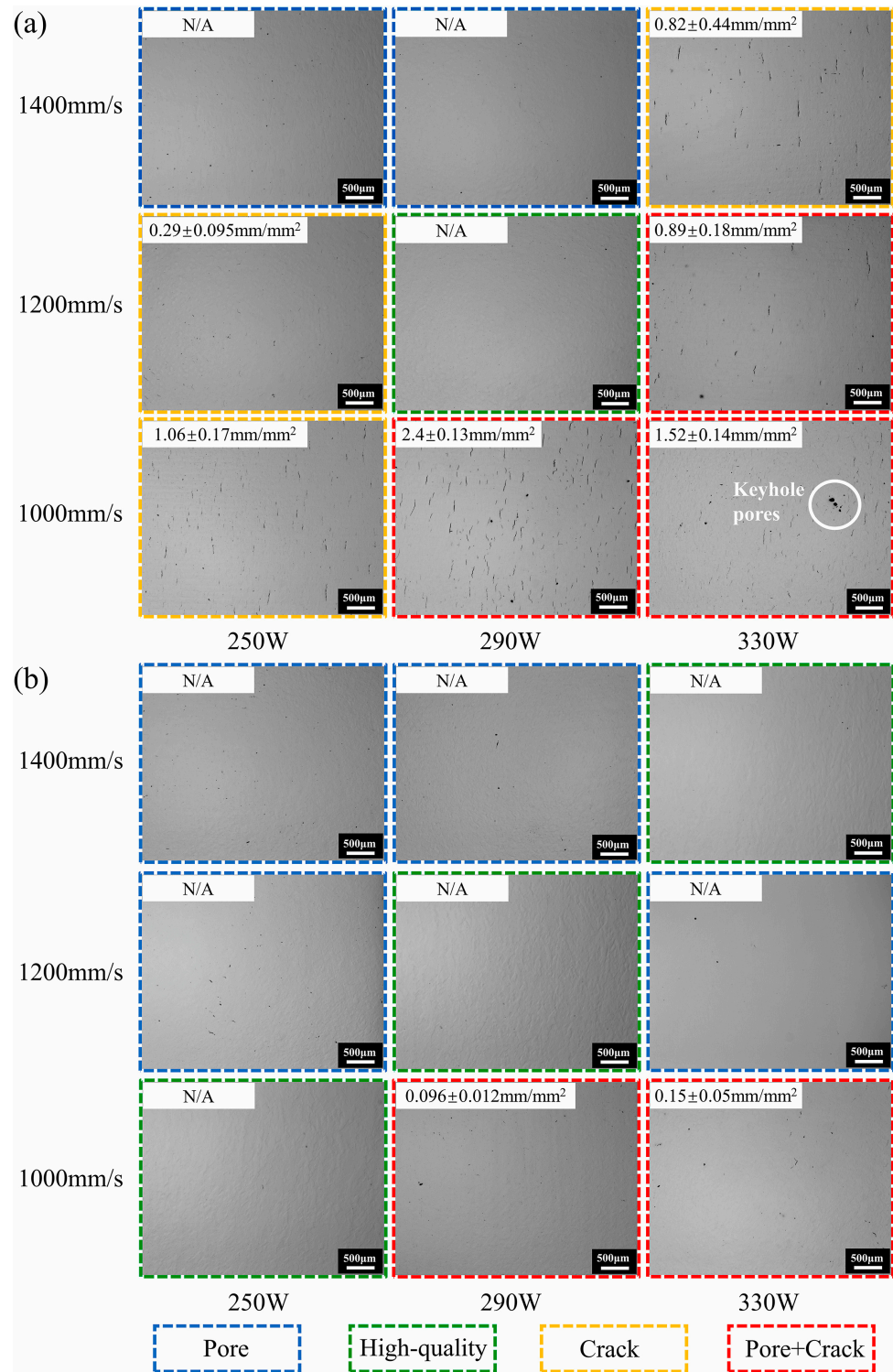


Figure 7. OM images of the polished surfaces of Inconel 738 alloy (a) without Y_2O_3 and (b) with Y_2O_3 fabricated by LPBF showing pore and crack under different laser powers and scan speeds as well as the corresponding crack density [57].

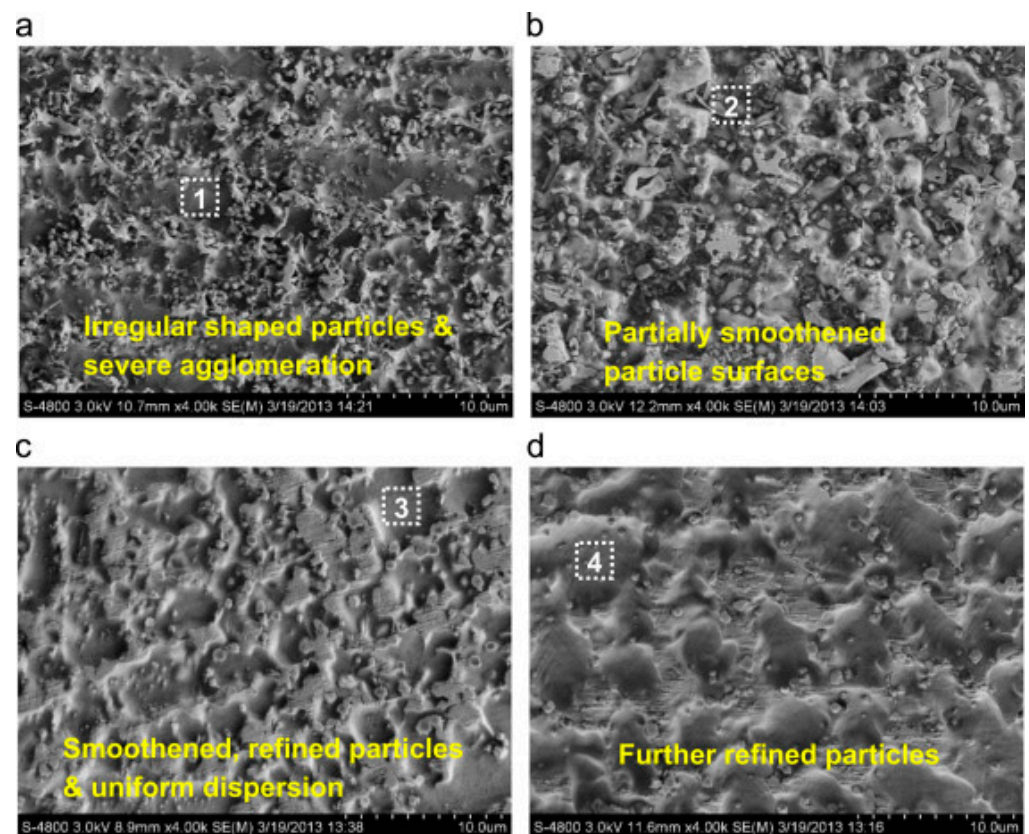


Figure 8. High-magnification SEM images showing composite structures of LMD-processed TiC/Inconel 625 parts using (a) $P = 500$ W, $v = 900$ mm/min, LEIPUL = 33 kJ/m; (b) $P = 800$ W, $v = 900$ mm/min, LEIPUL = 53 kJ/m; (c) $P = 500$ W, $v = 300$ mm/min, LEIPUL = 100 kJ/m; and (d) $P = 800$ W, $v = 300$ mm/min, LEIPUL = 160 kJ/m [67].

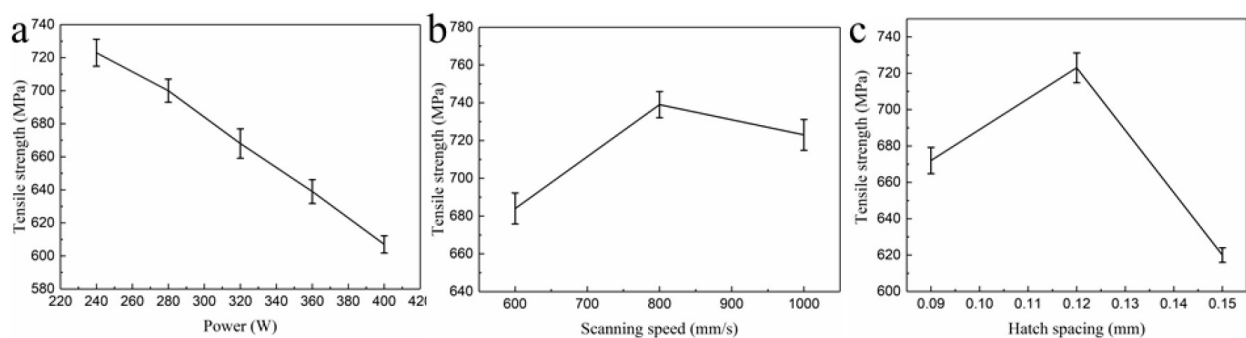


Figure 9. Effect of process parameters on the tensile strength: (a) power, (b) scanning speed, (c) hatch spacing [71].

In addition to process parameter optimizing for controlling manufacturing defect, it has been proved by a large number of studies that adding ceramic particles to the metal matrix is feasible to eliminate cracks forming during laser AM process. For example, Han et al. [72] investigated the effect of nano-TiC on the distribution of defects and molten pool boundaries in LBPBF Hastelloy X matrix composites. They found that TiC particles addition eliminated obviously pores and cracks in the molten pool in Hastelloy X alloy (Figure 10). The yield strength (830MPa) and UTS (1150MPa) of LBPBF TiC/Hastelloy X composite are much higher than that the yield strength (690MPa) and UTS (920MPa) of LBPBF Hastelloy X alloy. Cheng et al. [73] studied the effect of adding Y_2O_3 on cracks and mechanical properties of LBPBF Hastelloy X alloy. It can be seen from Figure 11a that many cracks (yellow arrows) were found in the LBPBF Hastelloy X alloy. The results showed that

the addition of Y_2O_3 eliminated the crack, and the microstructure uniformity of LBPBF Y_2O_3 /Hastelloy X composite was improved (Figure 11).

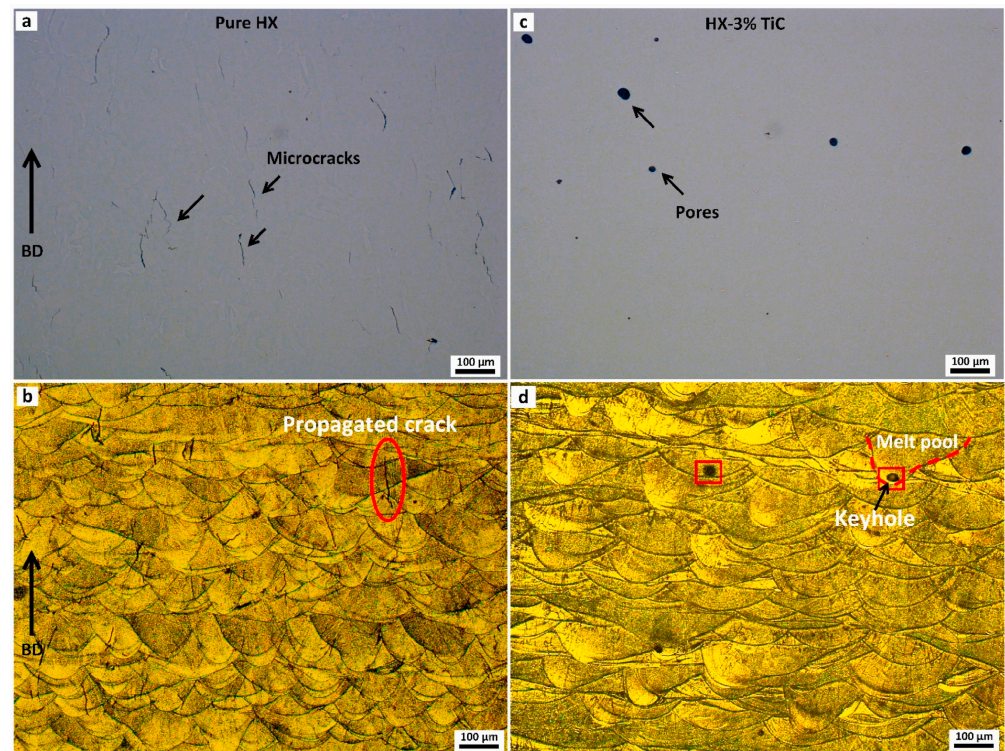


Figure 10. Defect distribution and molten pools in the built samples under optimum conditions: (a,b) Hastelloy X; (c,d) Hastelloy X matrix composite [72].

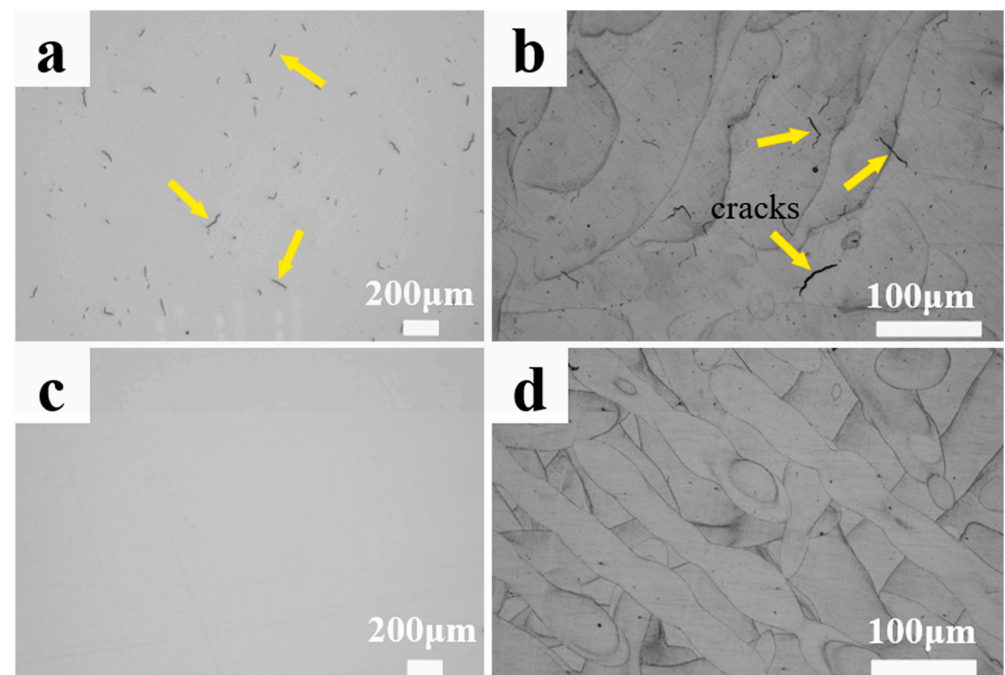


Figure 11. OM images of LBPBF manufactured specimens, (a,b) undoped specimen; (c,d) Y_2O_3 -doped specimen [73].

4. Strengthening Mechanism

It has been demonstrated that the strength of laser AM NAMMC is able to be enhanced by the reinforcement without sacrificing plasticity, which is mainly attributed to some strengthening synergy mechanism, such as stress-transfer strengthening, grain refinement strengthening, Orowan strengthening and high-density dislocation strengthening [69,74–76]. Wang et al. [77] studied the strengthening mechanism of LBPBF TiC/GTD222 composites. As can be seen from Figure 12a, the yield strength (1270 MPa) and UTS (1390MPa) of LBPBF TiC/GTD222 composite are much higher than the yield strength (831 MPa) and UTS (1100MPa) of LBPBF GTD222 alloy. This is mainly due to Orowan strengthening of TiC particles evenly dispersed in the cellular and columnar structures (Figure 12b). Both TiC and γ' phases prevent movable dislocations from moving (Figure 12). Yao et al. [78] deemed that the increased strength of TiC/IN718 composites alloy was mainly attributed to the combination of grain refinement strengthening and high-density dislocation strengthening. Zheng et al. [11] thought the strengthening mechanism of LENS TiC/IN625 composite was ascribed to a large number of dislocations around TiC particles (Figure 13), which was caused by the residual stress between the reinforcement TiC and the matrix IN625 alloy. Zhang et al. [5] considered that LBPBF TiC/GTD222 composite with high strength was concerned with the well-combined interface between matrix and TiC reinforcement (Figure 14a). The inset in Figure 14a shows the Fourier transform image of the carbide, and it can be identified as TiC particles. In addition, they found that there were a large number of dislocations (yellow symbols) at the interface between the matrix and the reinforcement due to the difference in lattice constants between matrix and the reinforcement (Figure 14b). Therefore, they believed that the increase in strength of TiC/GTD222 composite was attributed to the synergistic effect of load-bearing strengthening of particles and Orowan strengthening.

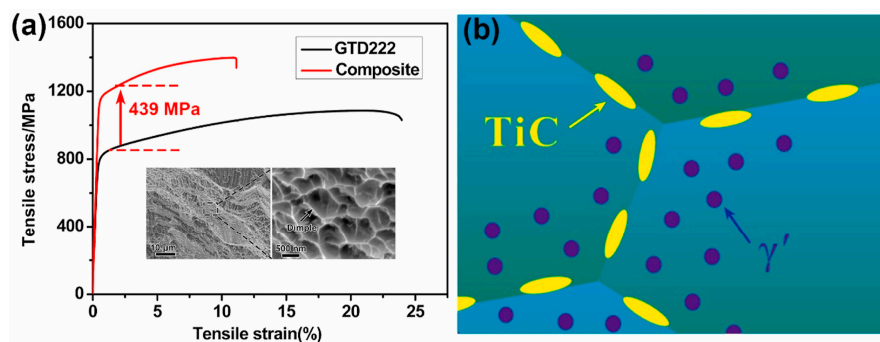


Figure 12. (a) Typical tensile stress-strain curves of LBPBF processed GTD222 alloy and TiC particle-reinforced Ni matrix composite; (b) schematic illustration of the strengthening mechanisms in TiC particle-reinforced Ni matrix composite [77].

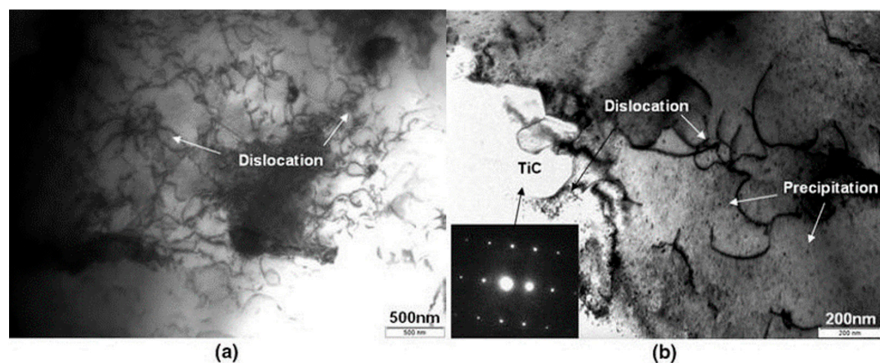


Figure 13. TEM micrographs of LENS-deposited IN625 TiC/Ni MMCs: (a) high density of dislocation in matrix and (b) large amount of precipitation interacting with dislocations [11].

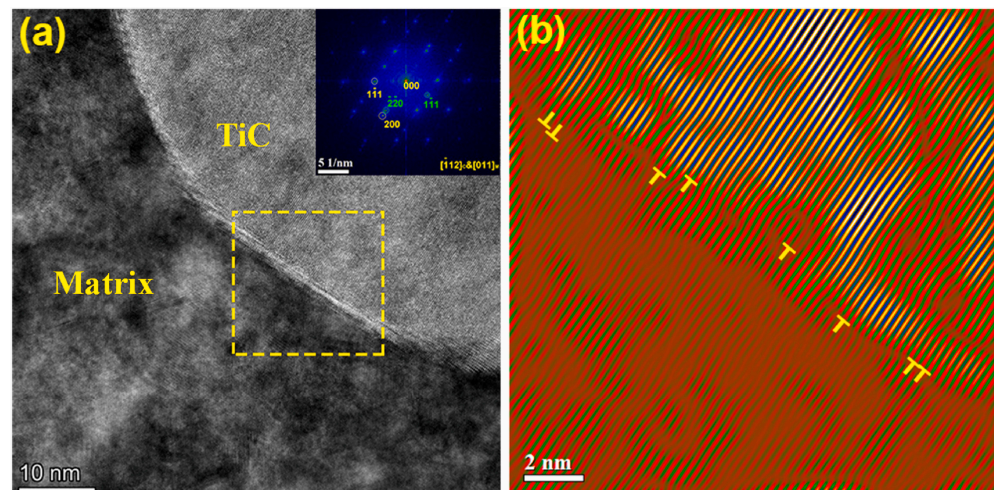


Figure 14. (a) Interfacial bonding of TiC particles and GTD222 matrix, (b) Dislocations (yellow symbols) [5].

5. Heat Treatment of Nickel-Based Alloy Composites

The extremely high melting and solidification rates of laser AM technologies result in high residual stresses of NAMMC parts [79–82]. In addition, NAMMC parts may undergo phase transitions or harmful phase precipitation at high temperatures, resulting in insufficient material strength and premature component failure in practical applications. Therefore, a subsequent heat treatment is required to eliminate residual stress and improve microstructure performance of the AM NAMMC. Zhang et al. [5] investigated the effect of heat treatment on the microstructure and mechanical properties of TiC/GTD222 nickel matrix composites prepared by LBPBF. Figure 15 shows the microstructure and the particle size distribution in GTD222 alloy and the TiC/GTD222 composite after heat treatment. It shows that the microstructures of both materials consist of γ matrix, γ' phase (black contrast) and carbide (bright contrast). It can be seen from Figure 15e,f that the average carbide size in GTD222 and the TiC/GTD222 composite after heat treatment are 123 nm and 125 nm, and the latter has more uniform carbide size distribution. In addition, the yield strength (1270 MPa) and UTS (1470 MPa) of the TiC/GTD222 composites are higher than the yield strength (1270 MPa) and UTS (1380 MPa) of the GTD222 alloy. However, the EI (8.1%) of the TiC/GTD222 composites is lower than that (15%) of the GTD222 alloy. Guo et al. [57] investigated the effect of heat treatment on the microstructure and mechanical properties of Y_2O_3 /IN738LC composites prepared by LBPBF. Figure 16a,b shows the microstructures of IN738LC alloy and Y_2O_3 /IN738LC composite after heat treatment, respectively. It is clearly seen from the figures that there are 2 groups of precipitates, i.e., coarse (red arrows) and fine precipitates (yellow arrows) in the microstructure. The coarse precipitates are primary γ' (400 nm), while the fine precipitates are secondary γ' (50 nm). The volume fractions of primary and secondary γ' for IN738LC alloy and Y_2O_3 /IN738LC composite are 36–38% and 24–26%, respectively. Figure 16c,d shows the inverse pole figures of the IN738LC alloy and the Y_2O_3 /IN738LC composite after heat treatment, respectively. The average grain size of the IN738LC alloy increased from 16.7 μm to 27.5 μm , and the average grain size of the Y_2O_3 /IN738LC composite increased from 19.9 μm to 29.3 μm after the heat treatment process. In addition, the yield strength (633 MPa) and UTS (773 MPa) of the Y_2O_3 /IN738LC composites are higher than the yield strength (615 MPa) and UTS (714 MPa) of the IN738LC alloy. However, the EI of the Y_2O_3 /IN738LC composites is slightly decreased.

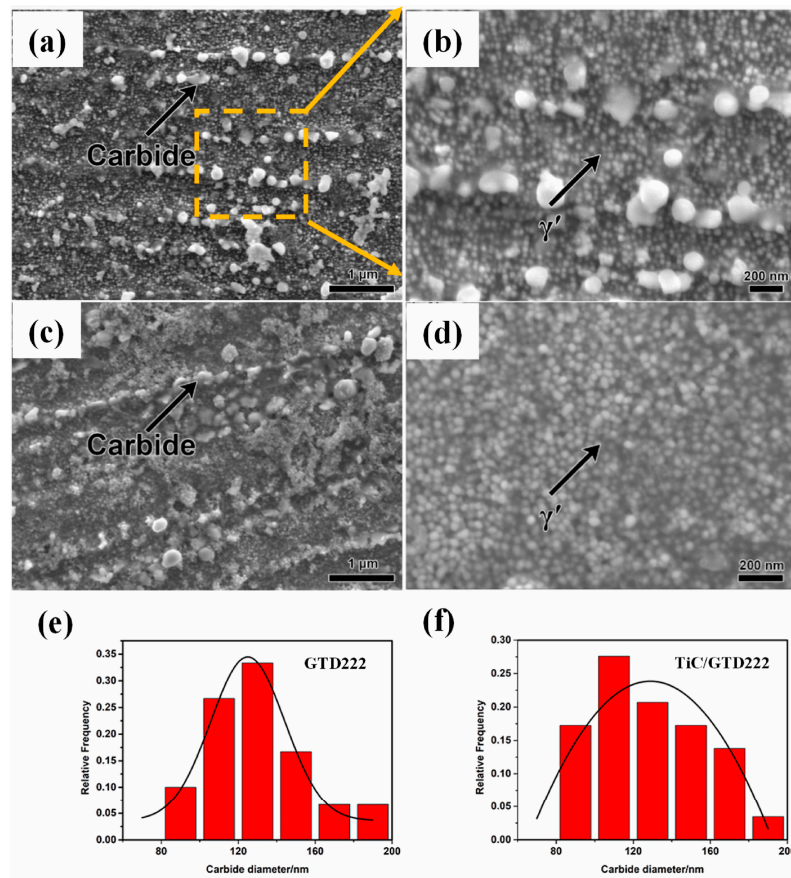


Figure 15. SEM images and corresponding to carbide particle size distributions after heat treatment: (a) GTD222, (b) Enlarged image of square area in Figure 14a, (c) TiC/GTD222 composite, (d) TiC/GTD222 local area magnification, (e) Carbide particle sizes distribution in GTD222, (f) Carbide particle sizes distribution in TiC/GTD222 composite [5].

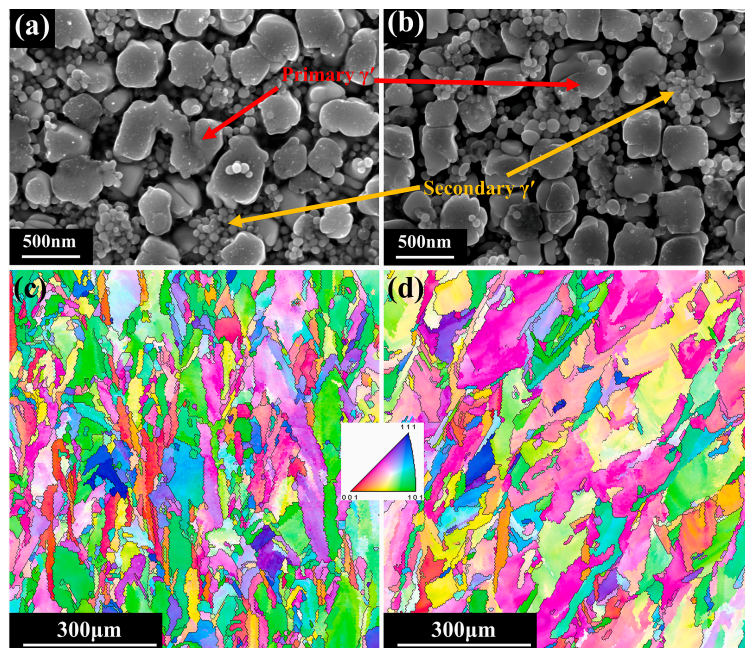


Figure 16. SEM images showing the microstructures (a) IN738LC alloy and (b) Y_2O_3 /IN738LC composite, EBSD mapping showing the grain structure of the (c) IN738LC alloy and (d) Y_2O_3 /IN738LC composite [57].

6. Conclusions and Prospect

In summary, due to the excellent high temperature strength, superior thermal fatigue resistance, high oxidation resistance and thermal corrosion resistance, the NAMMC is expected to replace traditional nickel-based alloys used in the manufacture of important hot-end components in aerospace, industrial gas turbines, seawater pipelines and other fields. It is well known that the future aerospace manufacturing industry requires more and more high temperature parts with complex structural designs. Using traditional manufacturing methods (forging and machining) to process these parts with complex internal and external profiles needs high-time cost and high-complexity complex process flow, and even some parts cannot be manufactured. From the above general description, high performance and complex structure parts of NAMMC was successfully fabricated using laser AM through a proper selection of reinforcement addition and process parameters. However, due to the large temperature gradient and extremely high cooling rate of laser AM process, high residual stress introduced deformation and cracking come out easily inside laser AM NAMMC. This problem should deserve a lot of attention of researchers. In addition, the traditional reinforcement addition improves the strength of the metal matrix at the price of sacrificing metal matrix plasticity as well as fracture toughness. Moreover, the microstructure stability of some reinforcement is deteriorated during long-term and high-temperature service. Therefore, the research and development of new reinforcement with stable crystal structure for improving strengthen and toughen synchronously is the great challenge of the field in the future.

Author Contributions: Conceptualization, S.G. and B.H.; methodology, Z.W.; software, S.L. and W.Z.; validation, S.G., B.H. and Y.J.; formal analysis, L.L.; investigation, Z.W.; resources, S.G.; data curation, L.L.; writing—original draft preparation, Z.W.; writing—review and editing, S.G.; visualization, Y.J.; supervision, B.H.; project administration, B.H.; funding acquisition, S.G. All authors have read and agreed to the published version of the manuscript.

Funding: This research was funded by Shanghai Sailing Program (No. 19YF1417500).

Institutional Review Board Statement: Not applicable.

Informed Consent Statement: Not applicable.

Data Availability Statement: Not applicable.

Conflicts of Interest: The authors declare no conflict of interest.

References

1. Dinda, G.P.; Dasgupta, A.K.; Mazumder, J. Laser Aided Direct Metal Deposition of Inconel 625 Superalloy: Microstructural Evolution and Thermal Stability. *Mater. Sci. Eng. A* **2009**, *509*, 98–104. [[CrossRef](#)]
2. Ma, D.; Stoica, A.D.; Wang, Z.; Beese, A.M. Crystallographic Texture in an Additively Manufactured Nickel-Base Superalloy. *Mater. Sci. Eng. A* **2017**, *684*, 47–53. [[CrossRef](#)]
3. Xu, F.; Lv, Y.; Liu, Y.; Shu, F.; He, P.; Xu, B. Microstructural Evolution and Mechanical Properties of Inconel 625 Alloy during Pulsed Plasma Arc Deposition Process. *J. Mater. Sci. Technol.* **2013**, *29*, 480–488. [[CrossRef](#)]
4. Gao, S.; Hou, J.; Yang, F.; Guo, Y.; Zhou, L. Effect of Ta on Microstructural Evolution and Mechanical Properties of a Solid-Solution Strengthening Cast Ni-Based Alloy during Long-Term Thermal Exposure at 700 °C. *J. Alloys Compd.* **2017**, *729*, 903–913. [[CrossRef](#)]
5. Zhang, Z.; Wang, R.; Lv, Y.; Liu, W.; Liu, Y. Microstructures and Mechanical Properties of Heat Treated TiC/GTD222 Nickel-Based Composite Prepared by Selective Laser Melting. *Mater. Sci. Eng. A* **2022**, *851*, 143588. [[CrossRef](#)]
6. Gu, D.; Zhang, H.; Dai, D.; Xia, M.; Hong, C.; Poprawe, R. Laser Additive Manufacturing of Nano-TiC Reinforced Ni-Based Nanocomposites with Tailored Microstructure and Performance. *Compos. Part B Eng.* **2019**, *163*, 585–597. [[CrossRef](#)]
7. Xia, T.; Wang, R.; Bi, Z.; Wang, R.; Zhang, P.; Sun, G.; Zhang, J. Microstructure and Mechanical Properties of Carbides Reinforced Nickel Matrix Alloy Prepared by Selective Laser Melting. *Materials* **2021**, *14*, 4792. [[CrossRef](#)] [[PubMed](#)]
8. Lan, L.; Xuan, W.; Wang, J.; Li, C.; Ren, Z.; Yu, J.; Peng, J. Interfacial Microstructure of Partial Transient Liquid Phase Bonding of Si 3 N 4 to Nickel-Base Superalloy Using Ti/Au/Ni Interlayers. *Vacuum* **2016**, *130*, 105–108. [[CrossRef](#)]
9. Zhang, H.; Gu, D.; Ma, C.; Guo, M.; Yang, J.; Zhang, H.; Chen, H.; Li, C.; Svyarenko, K.; Kosiba, K. Understanding Tensile and Creep Properties of WC Reinforced Nickel-Based Composites Fabricated by Selective Laser Melting. *Mater. Sci. Eng. A* **2021**, *802*, 140431. [[CrossRef](#)]

10. Kong, D.; Dong, C.; Ni, X.; Zhang, L.; Man, C.; Zhu, G.; Yao, J.; Yao, J.; Wang, L.; Cheng, X.; et al. Effect of TiC Content on the Mechanical and Corrosion Properties of Inconel 718 Alloy Fabricated by a High-Throughput Dual-Feed Laser Metal Deposition System. *J. Alloys Compd.* **2019**, *803*, 637–648. [[CrossRef](#)]
11. Zheng, B.; Topping, T.; Smugeresky, J.E.; Zhou, Y.; Biswas, A.; Baker, D.; Lavernia, E.J. The Influence of Ni-Coated TiC on Laser-Deposited IN625 Metal Matrix Composites. *Metall. Mater. Trans. A* **2010**, *41*, 568–573. [[CrossRef](#)]
12. Trosch, T.; Strößner, J.; Völkl, R.; Glatzel, U. Microstructure and Mechanical Properties of Selective Laser Melted Inconel 718 Compared to Forging and Casting. *Mater. Lett.* **2016**, *164*, 428–431. [[CrossRef](#)]
13. Song, Z.; Gao, S.; Wang, Z.; Lan, L.; Hou, J.; He, B. Effects of Non-Equilibrium Microstructures on Microstructure Evolution and Mechanical Properties of Laser Powder Bed Fusion IN625 Ni-Based Superalloy during Long-Term Thermal Exposure at 700 °C and 750 °C. *Mater. Sci. Eng. A* **2022**, *856*, 143883. [[CrossRef](#)]
14. Xu, J.; Kontis, P.; Peng, R.L.; Moverare, J. Modelling of Additive Manufacturability of Nickel-Based Superalloys for Laser Powder Bed Fusion. *Acta Mater.* **2022**, *240*, 118307. [[CrossRef](#)]
15. Bai, C.; Lan, L.; Xin, R.; Gao, S.; He, B. Microstructure Evolution and Cyclic Deformation Behavior of Ti-6Al-4 V Alloy via Electron Beam Melting during Low Cycle Fatigue. *Int. J. Fatigue* **2022**, *159*, 106784. [[CrossRef](#)]
16. Hwang, J.Y.; Lim, B.K.; Tiley, J.; Banerjee, R.; Hong, S.H. Interface Analysis of Ultra-High Strength Carbon Nanotube/Nickel Composites Processed by Molecular Level Mixing. *Carbon* **2013**, *57*, 282–287. [[CrossRef](#)]
17. Liu, Z.; Tian, J.; Li, B.; Zhao, L. Microstructure and Mechanical Behaviors of in Situ TiC Particulates Reinforced Ni Matrix Composites. *Mater. Sci. Eng. A* **2010**, *527*, 3898–3903. [[CrossRef](#)]
18. Song, Q.; Xu, Q.; Xu, L.; Ning, Z.; Lou, T.; Xie, H.; Qi, Y.; Yu, K. Synthesis of Ni-TiC Composite Powder Electrochemically in Molten Chlorides. *J. Alloys Compd.* **2017**, *690*, 116–122. [[CrossRef](#)]
19. Luu, D.N.; Zhou, W.; Nai, S.M.L.; Yang, Y. Mitigation of Solute Segregation during Solutionization of Selective Laser Melted Inconel 718 through Micron-TiC Addition. *J. Alloys Compd.* **2022**, *897*, 163224. [[CrossRef](#)]
20. Jia, Q.; Gu, D. Selective Laser Melting Additive Manufacturing of TiC/Inconel 718 Bulk-Form Nanocomposites: Densification, Microstructure, and Performance. *J. Mater. Res.* **2014**, *29*, 1960–1969. [[CrossRef](#)]
21. Shi, Q.; Zhong, G.; Sun, Y.; Politis, C.; Yang, S. Effects of Laser Melting+remelting on Interfacial Macroseggregation and Resulting Microstructure and Microhardness of Laser Additive Manufactured H13/IN625 Bimetals. *J. Manuf. Process.* **2021**, *71*, 345–355. [[CrossRef](#)]
22. Yang, S.; Han, Q.; Yin, Y.; Zhang, Z.; Wang, L.; Zhu, Z.; Liu, H.; Ma, T.; Gao, Z. Effects of TiB₂ Content on the Processability and Mechanical Performance of Hastelloy-X Based Composites Fabricated by Selective Laser Melting. *Opt. Laser Technol.* **2022**, *155*, 108441. [[CrossRef](#)]
23. Chen, L.; Sun, Y.; Li, L.; Ren, X. Effect of Heat Treatment on the Microstructure and High Temperature Oxidation Behavior of TiC/Inconel 625 Nanocomposites Fabricated by Selective Laser Melting. *Corros. Sci.* **2020**, *169*, 108606. [[CrossRef](#)]
24. Ao, M.; Liu, H.; Dong, C. The Effect of La₂O₃ Addition on Intermetallic-Free Aluminium Matrix Composites Reinforced with TiC and Al₂O₃ Ceramic Particles. *Ceram. Int.* **2019**, *45*, 12001–12009. [[CrossRef](#)]
25. Lakshmikanthan, A.; Bontha, S.; Krishna, M.; Koppad, P.G.; Ramprabhu, T. Microstructure, Mechanical and Wear Properties of the A357 Composites Reinforced with Dual Sized SiC Particles. *J. Alloys Compd.* **2019**, *786*, 570–580. [[CrossRef](#)]
26. Narayanasamy, R.; Ramesh, T.; Prabhakar, M. Effect of Particle Size of SiC in Aluminium Matrix on Workability and Strain Hardening Behaviour of P/M Composite. *Mater. Sci. Eng. A* **2009**, *504*, 13–23. [[CrossRef](#)]
27. Kumar, B.A.; Murugan, N.; Dinaharan, I. Dry Sliding Wear Behavior of Stir Cast AA6061-T6/AlNp Composite. *Trans. Nonferrous Met. Soc. China* **2014**, *24*, 2785–2795. [[CrossRef](#)]
28. Liu, Z.Y.; Kent, D.; Schaffer, G.B. Powder Injection Moulding of an Al–AlN Metal Matrix Composite. *Mater. Sci. Eng. A* **2009**, *513–514*, 352–356. [[CrossRef](#)]
29. Gao, X.; Wang, W.; Shang, F.; Liu, R.; Zhao, W.; Sun, T. Preparation and Interfacial Bonding of Oversize ZrO₂ Reinforced Metal Matrix Composites Prepared by Spark Plasma Sintering. *Mater. Lett.* **2022**, *329*, 133152. [[CrossRef](#)]
30. Umanath, K.; Palanikumar, K.; Selvamani, S.T. Analysis of Dry Sliding Wear Behaviour of Al6061/SiC/Al₂O₃ Hybrid Metal Matrix Composites. *Compos. Part B Eng.* **2013**, *53*, 159–168. [[CrossRef](#)]
31. Lei, J.; Shi, C.; Zhou, S.; Gu, Z.; Zhang, L.-C. Enhanced Corrosion and Wear Resistance Properties of Carbon Fiber Reinforced Ni-Based Composite Coating by Laser Cladding. *Surf. Coat. Technol.* **2018**, *334*, 274–285. [[CrossRef](#)]
32. Isaza Merino, C.A.; Ledezma Sillas, J.E.; Meza, J.M.; Herrera Ramirez, J.M. Metal Matrix Composites Reinforced with Carbon Nanotubes by an Alternative Technique. *J. Alloys Compd.* **2017**, *707*, 257–263. [[CrossRef](#)]
33. Geng, H.; Chen, B.; Wan, J.; Shen, J.; Kondoh, K.; Li, J.S. Matrix Effect on Strengthening Behavior of Carbon Nanotubes in Aluminum Matrix Composites. *Mater. Charact.* **2023**, *195*, 112484. [[CrossRef](#)]
34. Gao, Y.; Zou, J.; Wang, X.; Wang, X.; Yang, J.; Wang, H. Microstructure and Mechanical Performance of Graphene Nanosheets Reinforced Nickel-Based Superalloy FGH95 Composite. *Nanomaterials* **2020**, *10*, 100. [[CrossRef](#)] [[PubMed](#)]
35. Gao, Y.-X.; Zou, J.-W.; Wang, X.-F.; Yang, J.; Li, Z.; Zhu, Y.-Y.; Wang, H.-M. An Approach to the Uniform Dispersion of Graphene Nanosheets in Powder Metallurgy Nickel-Based Superalloy. *Materials* **2019**, *12*, 974. [[CrossRef](#)] [[PubMed](#)]
36. Wang, R.; Zhu, G.; Zhou, W.; Wang, W.; Wang, D.; Dong, A.; Shu, D.; Sun, B. An Enhanced Strength Ni Matrix Composite Reinforced by a 3D Network Structure of TiN Nano-Particles. *Mater. Des.* **2020**, *191*, 108638. [[CrossRef](#)]

37. Huang, L.J.; Geng, L.; Peng, H.-X. Microstructurally Inhomogeneous Composites: Is a Homogeneous Reinforcement Distribution Optimal? *Prog. Mater. Sci.* **2015**, *71*, 93–168. [[CrossRef](#)]
38. Shirvanimoghaddam, K.; Hamim, S.U.; Karbalaee Akbari, M.; Fakhrhoseini, S.M.; Khayyam, H.; Pakseresht, A.H.; Ghasali, E.; Zabet, M.; Munir, K.S.; Jia, S.; et al. Carbon Fiber Reinforced Metal Matrix Composites: Fabrication Processes and Properties. *Compos. Part Appl. Sci. Manuf.* **2017**, *92*, 70–96. [[CrossRef](#)]
39. Khoddamzadeh, A.; Liu, R.; Liang, M.; Yang, Q. Wear Resistant Carbon Fiber Reinforced Stellite Alloy Composites. *Mater. Des. 1980–2015* **2014**, *56*, 487–494. [[CrossRef](#)]
40. Sahoo, B.P.; Das, D.; Rath, P.; Chakrabarty, S.; Roy, S.; Mohanta, K. Improving Reinforcement Properties of CNTs in Aluminium Matrix Composites: A Case of Surface Modification through AlN Nano-Particle Grafting. *Surf. Interfaces* **2022**, 102571. [[CrossRef](#)]
41. Mallakpour, S.; Khadem, E. Carbon Nanotube–Metal Oxide Nanocomposites: Fabrication, Properties and Applications. *Chem. Eng. J.* **2016**, *302*, 344–367. [[CrossRef](#)]
42. Wang, M.; Zhao, Y.; Wang, L.-D.; Zhu, Y.-P.; Wang, X.-J.; Sheng, J.; Yang, Z.-Y.; Shi, H.-L.; Shi, Z.-D.; Fei, W.-D. Achieving High Strength and Ductility in Graphene/Magnesium Composite via an in-Situ Reaction Wetting Process. *Carbon* **2018**, *139*, 954–963. [[CrossRef](#)]
43. Zhou, W.; Yamaguchi, T.; Kikuchi, K.; Nomura, N.; Kawasaki, A. Effectively Enhanced Load Transfer by Interfacial Reactions in Multi-Walled Carbon Nanotube Reinforced Al Matrix Composites. *Acta Mater.* **2017**, *125*, 369–376. [[CrossRef](#)]
44. Yin, Y.; Zhang, J.; Gao, J.; Zhang, Z.; Han, Q.; Zan, Z. Laser Powder Bed Fusion of Ni-Based Hastelloy X Superalloy: Microstructure, Anisotropic Mechanical Properties and Strengthening Mechanisms. *Mater. Sci. Eng. A* **2021**, *827*, 142076. [[CrossRef](#)]
45. Zhang, B.; Bi, G.; Nai, S.; Sun, C.; Wei, J. Microhardness and Microstructure Evolution of TiB₂ Reinforced Inconel 625/TiB₂ Composite Produced by Selective Laser Melting. *Opt. Laser Technol.* **2016**, *80*, 186–195. [[CrossRef](#)]
46. Tan, C.; Ma, W.; Deng, C.; Zhang, D.; Zhou, K. Additive Manufacturing SiC-Reinforced Maraging Steel: Parameter Optimisation, Microstructure and Properties. *Adv. Powder Mater.* **2023**, *2*, 100076. [[CrossRef](#)]
47. Konopatsky, A.S.; Kvashnin, D.G.; Corthay, S.; Boyarintsev, I.; Firestein, K.L.; Orekhov, A.; Arkharova, N.; Golberg, D.V.; Shtansky, D.V. Microstructure Evolution during AlSi10Mg Molten Alloy/BN Microflake Interactions in Metal Matrix Composites Obtained through 3D Printing. *J. Alloys Compd.* **2021**, *859*, 157765. [[CrossRef](#)]
48. Xu, R.; Geng, Z.; Wu, Y.; Chen, C.; Ni, M.; Li, D.; Zhang, T.; Huang, H.; Liu, F.; Li, R.; et al. Microstructure and Mechanical Properties of In-Situ Oxide-Dispersion-Strengthened NiCrFeY Alloy Produced by Laser Powder Bed Fusion. *Adv. Powder Mater.* **2022**, *1*, 100056. [[CrossRef](#)]
49. Simões, S.; Viana, F.; Reis, M.; Vieira, M. Aluminum and Nickel Matrix Composites Reinforced by CNTs: Dispersion/Mixture by Ultrasonication. *Metals* **2017**, *7*, 279. [[CrossRef](#)]
50. Zhou, S.; Zhang, W.; Liu, M.; Ren, W.; Zhou, Q.; Wei, J.; Wu, P. Strength-Toughness Combination in Nickel Matrix Composites Reinforced by Hybrid Graphene Nanoplatelets-Titanium Diboride. *Carbon* **2023**, *201*, 1137–1148. [[CrossRef](#)]
51. Wang, P.; Zhang, B.; Tan, C.C.; Raghavan, S.; Lim, Y.-F.; Sun, C.-N.; Wei, J.; Chi, D. Microstructural Characteristics and Mechanical Properties of Carbon Nanotube Reinforced Inconel 625 Parts Fabricated by Selective Laser Melting. *Mater. Des.* **2016**, *112*, 290–299. [[CrossRef](#)]
52. Chen, Z.; Wei, P.; Zhang, S.; Lu, B.; Zhang, L.; Yang, X.; Huang, K.; Huang, Y.; Li, X.; Zhao, Q. Graphene Reinforced Nickel-Based Superalloy Composites Fabricated by Additive Manufacturing. *Mater. Sci. Eng. A* **2020**, *769*, 138484. [[CrossRef](#)]
53. Ding, Y.; Zhang, S.; Liu, J. Research Progress of Particulate Reinforced Nickel Matrix Composites. *FOUNDRY Technol.* **2014**, *35*, 1376–05.
54. Han, Q.; Gu, Y.; Gu, H.; Yin, Y.; Song, J.; Zhang, Z.; Soe, S. Laser Powder Bed Fusion of WC-Reinforced Hastelloy-X Composite: Microstructure and Mechanical Properties. *J. Mater. Sci.* **2021**, *56*, 1768–1782. [[CrossRef](#)]
55. Zhang, Z.; Han, Q.; Yang, S.; Yin, Y.; Gao, J.; Setchi, R. Laser Powder Bed Fusion of Advanced Submicrometer TiB₂ Reinforced High-Performance Ni-Based Composite. *Mater. Sci. Eng. A* **2021**, *817*, 141416. [[CrossRef](#)]
56. Wang, W.; Wang, S.; Chen, F.; Zhang, X.; Xu, Y. Microstructure and Mechanical Properties of Ti N/Inconel 718 Composites Fabricated by Selective Laser Melting. *ACTA Metall. Sin.* **2021**, *57*, 1018–1026. [[CrossRef](#)]
57. Guo, C.; Yu, Z.; Hu, X.; Li, G.; Zhou, F.; Xu, Z.; Han, S.; Zhou, Y.; Ward, R.M.; Zhu, Q. Y₂O₃ Nanoparticles Decorated IN738LC Superalloy Manufactured by Laser Powder Bed Fusion: Cracking Inhibition, Microstructures and Mechanical Properties. *Compos. Part B Eng.* **2022**, *230*, 109555. [[CrossRef](#)]
58. Cooper, D.E.; Blundell, N.; Maggs, S.; Gibbons, G.J. Additive Layer Manufacture of Inconel 625 Metal Matrix Composites, Reinforcement Material Evaluation. *J. Mater. Process. Technol.* **2013**, *213*, 2191–2200. [[CrossRef](#)]
59. Wang, R.; Wang, W.; Zhu, G.; Pan, W.; Zhou, W.; Wang, D.; Li, F.; Huang, H.; Jia, Y.; Du, D.; et al. Microstructure and Mechanical Properties of the TiN Particles Reinforced IN718C Composite. *J. Alloys Compd.* **2018**, *762*, 237–245. [[CrossRef](#)]
60. Hong, C.; Gu, D.; Dai, D.; Gasser, A.; Weisheit, A.; Kelbassa, I.; Zhong, M.; Poprawe, R. Laser Metal Deposition of TiC/Inconel 718 Composites with Tailored Interfacial Microstructures. *Opt. Laser Technol.* **2013**, *54*, 98–109. [[CrossRef](#)]
61. Wang, Y.; Shi, J. Effect of Post Heat Treatment on the Microstructure and Tensile Properties of Nano TiC Particulate Reinforced Inconel 718 by Selective Laser Melting. *J. Manuf. Sci. Eng.* **2020**, *142*, 051004. [[CrossRef](#)]
62. Jiang, D.; Hong, C.; Zhong, M.; Alkhatat, M.; Weisheit, A.; Gasser, A.; Zhang, H.; Kelbassa, I.; Poprawe, R. Fabrication of Nano-TiCp Reinforced Inconel 625 Composite Coatings by Partial Dissolution of Micro-TiCp through Laser Cladding Energy Input Control. *Surf. Coat. Technol.* **2014**, *249*, 125–131. [[CrossRef](#)]

63. Tan, C.; Zou, J.; Wang, D.; Ma, W.; Zhou, K. Duplex Strengthening via SiC Addition and In-Situ Precipitation in Additively Manufactured Composite Materials. *Compos. Part B Eng.* **2022**, *236*, 109820. [[CrossRef](#)]
64. Yu, W.H.; Sing, S.L.; Chua, C.K.; Kuo, C.N.; Tian, X.L. Particle-Reinforced Metal Matrix Nanocomposites Fabricated by Selective Laser Melting: A State of the Art Review. *Prog. Mater. Sci.* **2019**, *104*, 330–379. [[CrossRef](#)]
65. Li, X.P.; Ji, G.; Chen, Z.; Addad, A.; Wu, Y.; Wang, H.W.; Vleugels, J.; Van Humbeeck, J.; Kruth, J.P. Selective Laser Melting of Nano-TiB₂ Decorated AlSi10Mg Alloy with High Fracture Strength and Ductility. *Acta Mater.* **2017**, *129*, 183–193. [[CrossRef](#)]
66. Li, W.; Di, R.; Yuan, R.; Song, H.; Lei, J. Microstructure, Wear Resistance and Electrochemical Properties of Spherical/Non-Spherical WC Reinforced Inconel 625 Superalloy by Laser Melting Deposition. *J. Manuf. Process.* **2022**, *74*, 413–422. [[CrossRef](#)]
67. Hong, C.; Gu, D.; Dai, D.; Alkhatay, M.; Urban, W.; Yuan, P.; Cao, S.; Gasser, A.; Weisheit, A.; Kelbassa, I.; et al. Laser Additive Manufacturing of Ultrafine TiC Particle Reinforced Inconel 625 Based Composite Parts: Tailored Microstructures and Enhanced Performance. *Mater. Sci. Eng. A* **2015**, *635*, 118–128. [[CrossRef](#)]
68. Cao, S. *Laser Melting Deposition Processed TiC Reinforced Nickel-based Superalloy Composites: Process Control Mechanism and Trans-Scale Reinforcing Effect*; Nanjing University of Aeronautics and Astronautics: Nanjing, China, 2017.
69. AlMangour, B.; Baek, M.-S.; Grzesiak, D.; Lee, K.-A. Strengthening of Stainless Steel by Titanium Carbide Addition and Grain Refinement during Selective Laser Melting. *Mater. Sci. Eng. A* **2018**, *712*, 812–818. [[CrossRef](#)]
70. Chen, L.; Sun, Y.; Li, L.; Ren, Y.; Ren, X. In Situ TiC/Inconel 625 Nanocomposites Fabricated by Selective Laser Melting: Densification Behavior, Microstructure Evolution, and Wear Properties. *Appl. Surf. Sci.* **2020**, *518*, 145981. [[CrossRef](#)]
71. Wang, G.; Huang, L.; Liu, Z.; Qin, Z.; He, W.; Liu, F.; Chen, C.; Nie, Y. Process Optimization and Mechanical Properties of Oxide Dispersion Strengthened Nickel-Based Superalloy by Selective Laser Melting. *Mater. Des.* **2020**, *188*, 108418. [[CrossRef](#)]
72. Han, Q.; Gu, Y.; Huang, J.; Wang, L.; Low, K.W.Q.; Feng, Q.; Yin, Y.; Setchi, R. Selective Laser Melting of Hastelloy X Nanocomposite: Effects of TiC Reinforcement on Crack Elimination and Strength Improvement. *Compos. Part B Eng.* **2020**, *202*, 108442. [[CrossRef](#)]
73. Cheng, X.; Zhao, Y.; Qian, Z.; Wu, J.; Dong, J.; Ma, Z.; Liu, Y. Crack Elimination and Mechanical Properties Enhancement in Additive Manufactured Hastelloy X via In-Situ Chemical Doping of Y₂O₃. *Mater. Sci. Eng. A* **2021**, *824*, 141867. [[CrossRef](#)]
74. AlMangour, B.; Kim, Y.-K.; Grzesiak, D.; Lee, K.-A. Novel TiB₂-Reinforced 316L Stainless Steel Nanocomposites with Excellent Room- and High-Temperature Yield Strength Developed by Additive Manufacturing. *Compos. Part B Eng.* **2019**, *156*, 51–63. [[CrossRef](#)]
75. Zhai, W.; Zhou, W.; Nai, S.M.L. Grain Refinement and Strengthening of 316L Stainless Steel through Addition of TiC Nanoparticles and Selective Laser Melting. *Mater. Sci. Eng. A* **2022**, *832*, 142460. [[CrossRef](#)]
76. Chen, H.; Lu, T.; Wang, Y.; Liu, Y.; Shi, T.; Prashanth, K.G.; Kosiba, K. Laser Additive Manufacturing of Nano-TiC Particles Reinforced CoCrFeMnNi High-Entropy Alloy Matrix Composites with High Strength and Ductility. *Mater. Sci. Eng. A* **2022**, *833*, 142512. [[CrossRef](#)]
77. Wang, R.; Zhu, G.; Yang, C.; Zhou, W.; Wang, D.; Dong, A.; Shu, D.; Sun, B. Novel Selective Laser Melting Processed In-Situ TiC Particle-Reinforced Ni Matrix Composite with Excellent Processability and Mechanical Properties. *Mater. Sci. Eng. A* **2020**, *797*, 140145. [[CrossRef](#)]
78. Yao, X.; Moon, S.K.; Lee, B.Y.; Bi, G. Effects of Heat Treatment on Microstructures and Tensile Properties of IN718/TiC Nanocomposite Fabricated by Selective Laser Melting. *Int. J. Precis. Eng. Manuf.* **2017**, *18*, 1693–1701. [[CrossRef](#)]
79. Liu, F.; Lin, X.; Yang, G.; Song, M.; Chen, J.; Huang, W. Microstructure and Residual Stress of Laser Rapid Formed Inconel 718 Nickel-Base Superalloy. *Opt. Laser Technol.* **2011**, *43*, 208–213. [[CrossRef](#)]
80. Měsíček, J.; Čegan, T.; Ma, Q.-P.; Halama, R.; Skotnicová, K.; Hajnyš, J.; Juřica, J.; Krpec, P.; Pagáč, M. Effect of Artificial Aging on the Strength, Hardness, and Residual Stress of SLM AlSi10Mg Parts Prepared from the Recycled Powder. *Mater. Sci. Eng. A* **2022**, *855*, 143900. [[CrossRef](#)]
81. Vinodh, K.; Tigga, A.K.; Barad, S. Influence of Post-Processing Techniques on Residual Stresses of SLM Processed HPNGV. *J. Manuf. Process.* **2021**, *66*, 189–197. [[CrossRef](#)]
82. Tridello, A.; Fiochi, J.; Biffi, C.A.; Chiandussi, G.; Rossetto, M.; Tuissi, A.; Paolino, D.S. Effect of Microstructure, Residual Stresses and Building Orientation on the Fatigue Response up to 109 Cycles of an SLM AlSi10Mg Alloy. *Int. J. Fatigue* **2020**, *137*, 105659. [[CrossRef](#)]

Disclaimer/Publisher's Note: The statements, opinions and data contained in all publications are solely those of the individual author(s) and contributor(s) and not of MDPI and/or the editor(s). MDPI and/or the editor(s) disclaim responsibility for any injury to people or property resulting from any ideas, methods, instructions or products referred to in the content.